PAPER

Check for updates

A graphene oxide coated tapered microfiber acting as a super-sensor for rapid detection of SARS-CoV-2†

Hao Jia, [iD] ‡*[ab] Ao Zhang,‡[c] Yuquan Yang,[a] Yaqi Cui,[a] Jianrong Xu,[a] Hewei Jiang,[d] Shengce Tao,[d] Dawei Zhang,[c] Heping Zeng,[e] Zhaoyuan Hou*[ab] and Jijun Feng*[c]

COVID-19 is a new strain of highly contagious coronavirus, and at present, more than 221.4 million people have been infected with this virus, and the death toll exceeds 2793398. Early and fast detection of COVID-19 from infected individuals is critical to limit its spreading. Here, we report an innovative approach to detect the severe acute respiratory syndrome coronavirus 2 (SARS-CoV-2) nucleocapsid (N) protein by combining DNA/RNA oligomers as aptamers and a graphene oxide (GO) coated optical microfiber as a sensor system. The DNA/RNA aptamers can effectively capture the SARS-CoV-2 N protein *in vitro*, with the GO coated optical microfiber aptasensor for real-time monitoring of the SARS-CoV-2 N protein. Due to the extremely high surface-to-volume ratio and excellent optical and biochemical properties of the GO surface layer, the fixing effect of the microfiber surface is significantly improved and the lowest limit of detection (LOD) is 6.25×10^{-19} M. Furthermore, in order to prove the feasibility of this sensing method in clinical applications, we use this sensor to detect the N protein mixed in fetal bovine serum (FBS) samples. The experimental results show that the biosensor can quickly and effectively detect the N protein (1×10^{-9} M) in a complex sample matrix within 3 minutes. These findings suggest that this approach can be utilized for quantitative monitoring of coronavirus particles due to its high sensitivity, which can help to quickly exclude patients who do not have the infection. Collectively, the optical microfiber sensor system could be expected to become an important platform for the diagnosis of coronavirus due to its simple detection scheme and easy miniaturization.

[a] *Faculty of Basic Medicine, Shanghai Jiaotong University School of Medicine, Shanghai, 200025, China. E-mail: fonney@sjtu.edu.cn; Tel: +86 18801901422*
[b] *Shanghai Key Laboratory for Tumor Microenvironment and Inflammation, Shanghai Jiaotong University School of Medicine, Shanghai, 200025, China. E-mail: houzy@sjtu.edu.cn; Tel: +86 15121148204*
[c] *Shanghai Key Laboratory of Modern Optical System, Engineering Research Center of Optical Instrument and System (Ministry of Education), School of Optical-Electrical and Computer Engineering, University of Shanghai for Science and Technology, Shanghai 200093, China. E-mail: fjijun@usst.edu.cn; Tel: +86 13917961036*
[d] *Shanghai Center for Systems Biomedicine, Key Laboratory of Systems Biomedicine (Ministry of Education), Shanghai Jiao Tong University, 200240, Shanghai, China*
[e] *State Key Laboratory of Precision Spectroscopy, East China Normal University, Shanghai 200062, China*
† Electronic supplementary information (ESI) available. See DOI: 10.1039/d0lc01231a
‡ These authors contributed equally to this work.

Introduction

Since the emergence of COVID-19 in late 2019, the third serious pandemic caused by coronavirus, COVID-19 (Coronavirus Disease-2019) has given rise to over 221.4 million confirmed cases and more than 2.793 million fatalities up to March 29, 2021. With the non-specific symptoms and signs of severe acute respiratory syndrome (SARS) and the long incubation period, COVID-19 appears to spread efficiently and unconsciously in people. To hold back the spread of the virus, it is crucial to develop a comprehensive understanding of the structure of severe acute respiratory syndrome coronavirus 2 (SARS-CoV-2) and to apply this knowledge towards developing an early detection system for suspected cases.[1] Classical SARS-CoV-2 tests involve nucleic acid testing and antibody detection.[2] However, current methods for nucleic acid and antibody detection have limitations. First, the availability of PCR reagent kits has not kept up with demand. Second, community hospitals outside of urban cities lack the PCR infrastructure to accommodate high sample throughput. Lastly, RT-PCR relies on the presence of detectable SARS-CoV-2 in the sample collected. If an asymptomatic patient was infected with SARS-CoV-2 but has recovered, PCR would not identify this prior infection, and control measures would not be enforced.[2] Antibodies in response to viral protein antigens of SARS-CoV-2 can also be used for diagnosing COVID-19. Xiang *et al.* tested specific IgM

and IgG antibodies in the patients confirmed with COVID-19 and in patients with suspected COVID-19, and found that the antibodies against SARS-CoV-2 can be detected in the middle and later stage of the illness.[3] However, it should be noted that the time needed for the reaction of body's immune system and potential cross-reactivity of SARS-CoV-2 antibodies with antibodies generated against other coronaviruses is usually very long.

A tapered optical fiber sensor is an excellent candidate for sensing.[4] Single-mode biconical tapered fibers can be applied as physical sensors for measurements of temperature,[5] displacement,[6] refractive index,[7,8] etc. Recently, many exciting researches on biological testing have been reported.[9] Li and his co-workers realized the detection of alpha-fetoprotein (AFP) with optical microfibers functionalized with special antibodies as low as 0.2 ng mL^{-1}.[10] Yep et al. proposed an interferometric optical microfiber sensor functionalized with nitrogen- and sulfur-codoped carbon dots (CDs) for the detection of ferric ions (Fe^{3+}) in biological samples, with a sensitivity of 0.0061 nm µg^{-1} L and a detection limit of 0.77 µg L^{-1}.[11] Xiao and his associates proposed an optical microfiber sensor functionalized with a polystyrene@gold nanosphere, which can detect trace carcinoembryonic antigen (CEA)-related cell adhesion molecules 5 (CEACAMs$_5$) in serum at the early stage.[12] The limit of detection (LOD) of the sensor can reach 3.54×10^{-17} M in pure solution and 5.27×10^{-16} M in serum with a sensitivity of 0.1 nm ng^{-1} mL. Optical microfiber sensors could be expected to become an important platform for the diagnosis of coronavirus due to its simple detection scheme and easy miniaturization. Moreover, graphene oxide (GO) is often used to improve the sensitivity of biosensors.[13,14] The GO linking layer can modify the surface of the optical fiber and introduce functional groups to immobilize bioreceptors on the surface, providing a remarkable analytical platform for bioaffinity binding interfaces.

Here in this paper, we describe a novel method for fast detection of the N protein of SARS-CoV-2 with extreme sensitivity. By combining DNA aptamers (DNA-AP) and RNA aptamers (RNA-AP) for specifically capturing the N protein and graphene oxide (GO) coated optical microfibers for sensing the N protein in solution, the LOD can reach as low as 6.25×10^{-19} M. Furthermore, we use this sensor to detect the N protein mixed in fetal bovine serum (FBS) samples. The experimental results show that the biosensor can quickly and effectively detect the N protein (1×10^{-9} M) in a complex sample matrix within 3 minutes. The optical microfiber sensor system could be expected to become an important platform for the diagnosis of coronavirus due to its simple detection scheme and easy miniaturization.

Materials and methods

Materials

The related chemical materials are sulfuric acid (H$_2$SO$_4$), hydrogen peroxide (H$_2$O$_2$), 3-aminopropyltriethoxysilane (APTES), ethanol (C$_2$H$_6$O), graphene oxide (GO), and deionized (DI) water. All chemical and biochemical reagents were of analytical grade and used as received without further purification. All aqueous solutions were prepared with DI water. The silica single-mode fiber (SMF-28, cladding diameter 125 µm) was purchased from Corning.

Plasmid and protein preparation

Plasmid His-SARS-CoV-2 N was previously described.[15] The recombinant His-SARS-CoV-2 N was expressed in E. coli BL21 cells under the treatment of 0.2 mM isopropyl-β-D-thiogalactoside (IPTG) at 16 °C overnight. The cell pellets were resuspended in a lysis buffer containing 50 µmM Tris-HCl (pH 8.0), 500 µmM NaCl and 20 µmM imidazole (pH 8.0). The supernatants were purified with Ni^{2+} Sepharose beads, washed with a lysis buffer, and eluted with a buffer containing 50 µmM Tris-HCl (pH 8.0), 500 µmM NaCl, and 300 µmM imidazole (pH 8.0).

EMSA measurement

Electrophoretic mobility shift assays (EMSAs) were performed using a LightShift Chemiluminescent EMSA Kit (20148). The 5′-biotin labeled RNA and DNA aptamers were incubated with increasing amounts of the N protein in a total volume of 8 µl of binding buffer. Unlabeled competitor aptamer RNA and DNA aptamers were used in the competition assays.

SPR assay

Surface plasmon resonance (SPR) analysis experiments were performed using a BIAcore T200 biosensor system to measure the binding affinity of selected aptamers. The carboxymethylated sensor chip (Cytiva) was pre-equilibrated with a running buffer (10 mM HEPES, pH 7.5, 150 mM NaCl, 1 mM MgCl$_2$, 1 mM CaCl$_2$, 2.7 mM KCl) and activated with 100 mM N-hydroxysuccinimide and 400 mM of N-ethyl-N′-(dimethylaminopropyl) carbodiimide to immobilize the His-tagged N protein on the chip surface. After the immobilization of the protein, the chip surface was deactivated with 1 M ethanolamine hydrochloride, pH 8.5, to block the remaining activated groups. After stabilizing the baseline, at least five different concentrations of the selected RNA/DNA aptamers were injected into the flow cells. The protein surface was regenerated with 10 mM NaOH after the injection of each sample and re-equilibrated with the running buffer. The SPR sensorgrams were analyzed to calculate the association rate constant k_a and the dissociation rate constant k_d using the BIAevaluation software (version 3.2, BIAcore).

Graphene oxide functionalized tapered fiber

The tapered microfibers with a waist diameter of 9.0 and 7.8 µm were fabricated, respectively, by the fusion method (Fig. S1†). They were made by heating the fibers locally and stretching both ends at the same time in the molten state.

Due to the obvious changes in their structure and size, the propagation characteristics of light in the optical fibers would be different accordingly.[16] The surface of the silica microfibers was aminated by sequential modifications with a piranha solution and APTES solution, which was then rich in positive charges, as shown in Fig. 1A.[17,18] Then, the modified fiber was coated with GO.[19] Through the electrostatic attraction between the oxygen-containing groups on GO and the amino group on the superfine fiber, it was functionalized on the surface of the silica microfiber.[20] Thus, the microfiber functionalized with graphene oxide could be obtained.

The microfiber surface without any functionalization was imaged by atomic force microscopy (AFM), with a scanning area of 5 μm × 5 μm as shown in Fig. 1B, compared with the rough microfiber surface. The root mean square (RMS) values of surface roughness are 0.12 and 5.93 nm, demonstrating the successful construction of the GO nanointerface on the silica microfiber.[21] Moreover, the Raman spectra in Fig. 1C and the energy dispersive X-ray (EDX) spectrum in Fig. 1D can also prove the functionalization on the surface of the silica microfibers. Next, the RNA and DNA aptamers were fixed on the optical fibers, respectively, and the RMS values of surface roughness are 31.49 and 52.78 nm, so that the

microfiber probes could be used for the monitoring of the SARS-CoV-2 N protein. The experimental setup is shown in Fig. 1E.

Results

Expression and purification of the SARS-CoV-2 N protein and selection of RNA/DNA aptamers

The same as other coronaviruses, the SARS-CoV-2 genome encodes four structural proteins called spike (S), envelope (E), membrane (M), and nucleocapsid (N). The N protein retains the RNA genome, while the S, E, and M proteins together form the viral envelope. The corresponding nucleotide sequences of N was cloned into a His-tagged vector and SDS-PAGE, showing that the purified and expressed proteins had good specificity (Fig. 2A). It was found that the N protein was 49 kDa, which was in accordance with the previous report. The N protein is a highly immunogenic phosphoprotein, and it is normally very conserved. The gene sequence of the N protein in SARS-CoV-2 is greater than 90% similar to that of the SARS-CoV nucleocapsid protein, and it has a great potential value for the diagnosis of the virus (Fig. 2B). Based on similar types of N protein, we searched
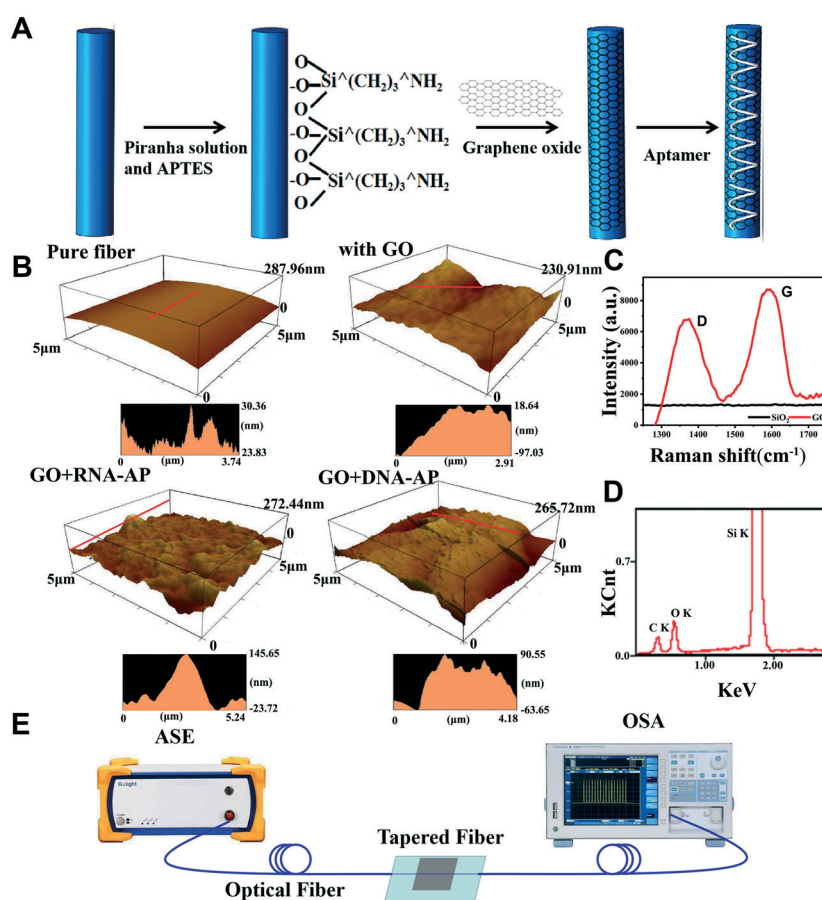

Fig. 1 (A) Scheme of the functionalization of the microfiber probe system. (B) AFM images of the pure optical fiber, which was coated with GO, RNA-AP@GO and DNA-AP@GO. (C) Raman spectra of the microfiber surfaces. (D) EDX spectrum of the microfiber with a GO nanointerface. (E) Schematic of the optical setup.
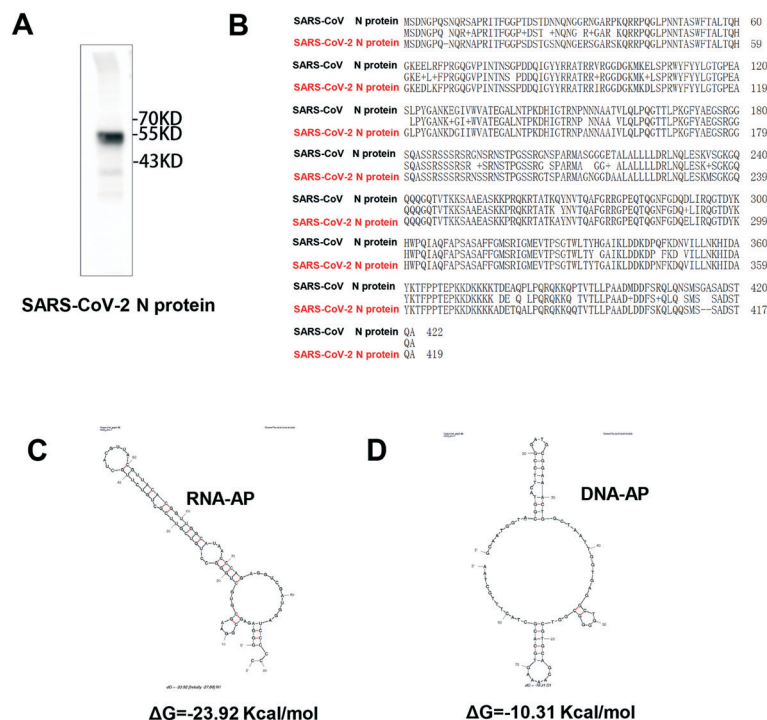
Fig. 2 (A) Western-blot assay of the purified N protein by SDS-PAGE. (B) Multiple sequence alignment and analysis of the SARS-CoV-1 N protein (UniProtKB P59595) and SARS-CoV-2 N protein (UniProtKB P0DTC9). The alignment was done using the CLUSTAL W2 program. (C) and (D) Sequences and secondary structures of RNA-AP and DNA-AP that bind to the N protein. The most stable secondary structures of the selected aptamers were predicted using the Mfold program.

the literature to screen out the best RNA and DNA aptamers of the SARS-CoV N protein for subsequent detection.[22,23] RNA-AP and DNA-AP secondary structures of the selected aptamers were analyzed using the Mfold program (Fig. 2C and D).[24]

Specific binding of RNA-AP and DNA-AP to the SARS-CoV-2 N protein

To assess the binding specificity of the RNA/DNA aptamers to the N protein, we performed EMSA. EMSA analyses were used

to evaluate the binding affinity of the RNA-AP (Fig. 3A) and DNA-AP (Fig. 3B) with the N protein, respectively. The color density of the electrophoretic bands corresponding to the RNA-AP (Fig. 3A) and DNA-AP (Fig. 3B) bound N proteins increases with increasing concentration of N protein. This result indicates that the RNA-AP/DNA-AP have a highly specific affinity to N protein. The binding ability of the selected RNA-AP/DNA-AP were further assessed by SPR assay. The SPR experiments reveal that the RNA-AP and DNA-AP bound strongly to the N protein, with an equilibrium dissociation constant (K_D) of 33.4 nM for RNA-AP (Fig. 4A)
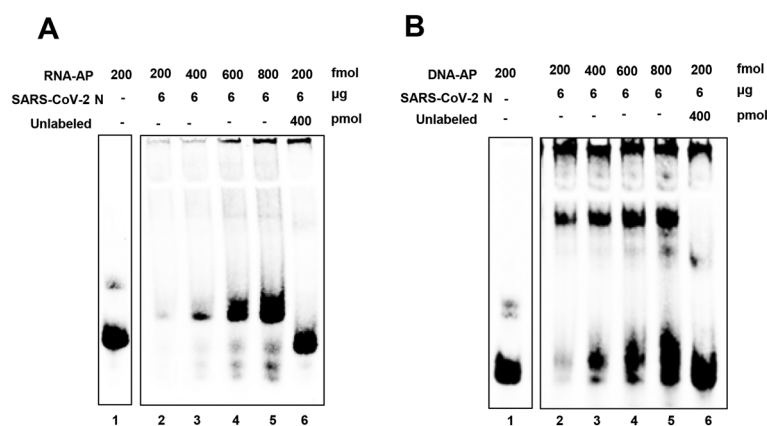

Fig. 3 EMSA was performed with the indicated (A) RNA-AP and (B) DNA-AP, which were incubated with increasing amounts of RNA-AP and DNA-AP (lanes 2–5; 200, 400, 600, and 800 fmol) to form aptamer/protein complexes.
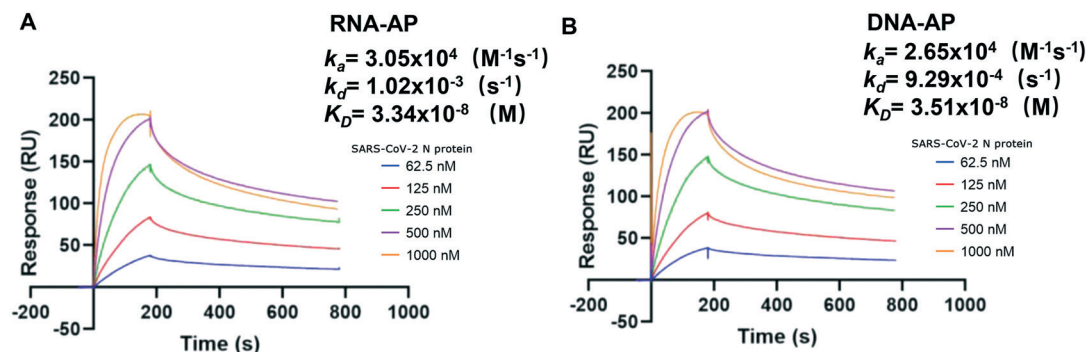
Fig. 4 Binding affinity of RNA-AP and DNA-AP to the SARS-CoV-2 N protein. Binding affinity determination for (A) RNA-AP and (B) DNA-AP, showing the spectra of the two aptamers.

and 35.1 nM for DNA-AP (Fig. 4B). Taken together, these results suggest that the RNA-AP and DNA-AP bind to the N protein with high specificity.

Detection of the SARS-CoV-2 N protein

The detection capability for the N protein pair of the two probes RNA-AP and DNA-AP with different optical microfiber aptasensors prepared was evaluated and the control experiments were carried out (more details are shown in Fig. S2 in the ESI†). The scanning electron microscopy images of the microfiber surface before and after the functionalization of the APs/GO interface are shown in Fig. 5. After covering the RNA-AP probes on the GO modified optical fiber, and then exposing them to N protein solution with concentrations varying from 10^{-18} to 10^{-7} M, the sensor showed obvious spectral modulation. As the concentration of the N protein solution increased, the transmission dip of the spectrum red-shifts obviously, showing a sensitivity of 1.21

nm log M^{-1} and a fitting linearity of 98.39% (Fig. 6A). It is worth noting that the LOD of the sensor is 6.25×10^{-18} M. Such a low LOD can facilitate trace analysis of the N protein.

Similarly, when the DNA-AP probes were connected with the GO modified optical fiber and exposed to an N protein solution with concentrations varying from 10^{-19} to 10^{-7} M, similar red-shifts of the spectrum transmission dip can be observed, with a sensitivity of 1.29 nm log M^{-1} and a fitting linearity of 99.08%, and the LOD is 6.25×10^{-19} M (Fig. 6B).

Due to the lack of sensitivity and selectivity of the silica microfibers to the N protein, the effect of nanointerfaces on the silica microfibers was also estimated. As a control experiment, an interface sensor without the GO nanointerface functionalized microfiber aptasensor was used. After the sensor was covered with the RNA-AP probe on a non-GO modified optical fiber, only protein solutions with a concentration of 10^{-15} M can be detected, showing a high LOD (Fig. 6C). Meanwhile, the sensor covered with the DNA-AP probe on the fiber without GO modification has an irregular frequency shift of the transmission dip (Fig. 6D), showing a poor spectral modulation. Clearly, the spectral red-shift effect is more obvious in the case of the GO nanointerface, which plays an important role in the sensitivity improvement.

Sensor response time for the SARS-CoV-2 N protein

To investigate the sensor response time, three SARS-CoV-2 N protein solutions with varying concentrations of 10^{-15}, 10^{-13}, and 10^{-9} M were tested using the same sensor probe.[25,26] The protein solutions with different concentrations were dropped into the microfiber, and the spectra were scanned and recorded every 20 s (limited by the optical spectrum analyzer). The relationship between the spectrum valley wavelength shift and the time is shown in Fig. 7. It can be seen that the spectra can stabilize after 20 s, which is the minimum detection time. With consideration of the time for sample dropping, the detection time is assumed to be about 3 min at most.

Selectivity of the sensor

Although the sensor aptamer can target the N protein, interfering molecule fluctuations in the extracellular
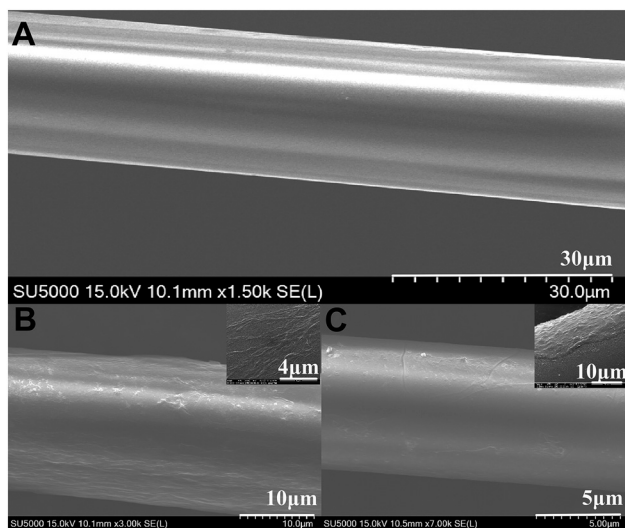

Fig. 5 SEM images of the optical fibers under different conditions: (A) clean, (B) GO nanointerface functionalized and (C) the aptamer incubated.
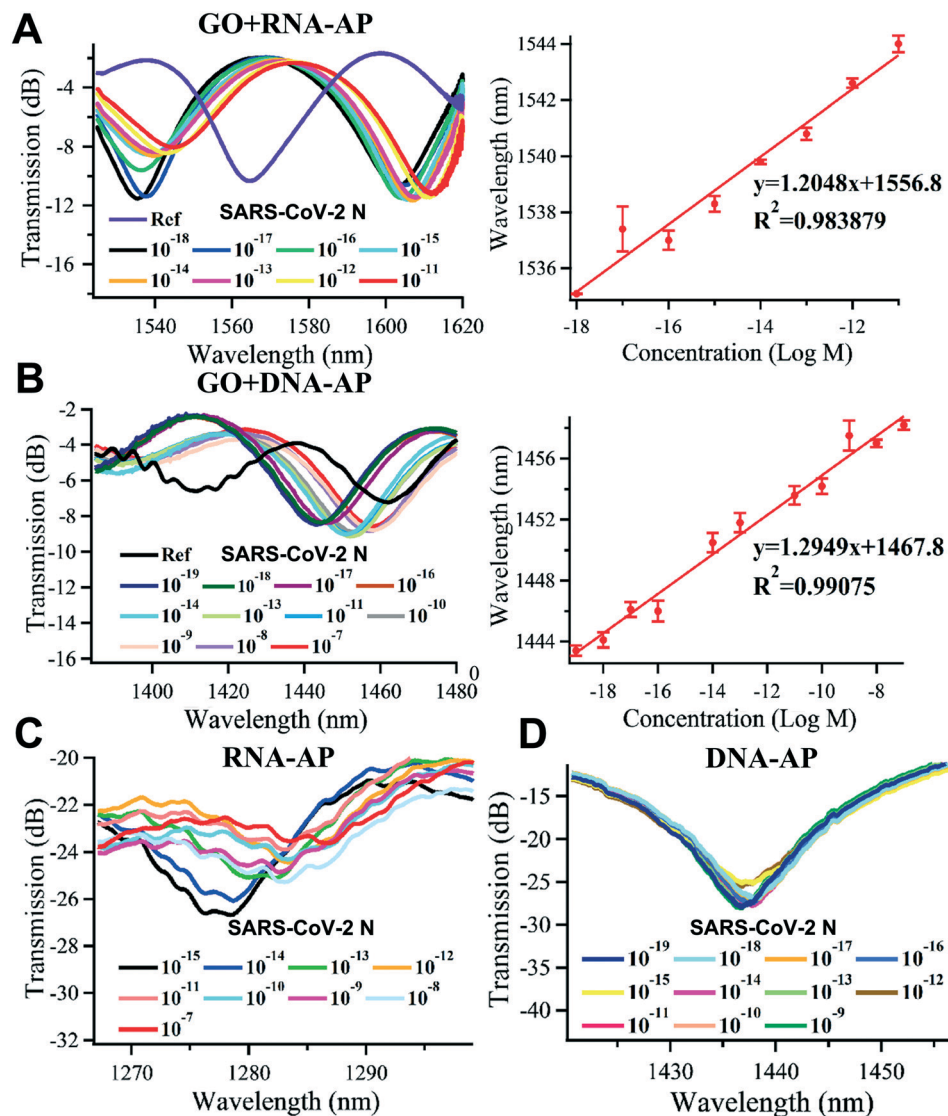
Fig. 6 (A) Left: transmission spectra of the RNA-AP fixed on the GO modified optical fiber. Right: wavelength and concentration corresponding to left. (B) Left: transmission spectra of the DNA-AP probe fixed on the GO modified optical fiber. Right: wavelength and concentration corresponding to left. (C) Transmission spectra of the RNA-AP probe fixed on the non-GO modified optical fiber. (D) Transmission spectra of the DNA-AP probe fixed on the non-GO modified optical fiber.

environment are inevitable in the real detection environment, which should be considered and discussed in the detection conditions. In order to reflect the physiological conditions in
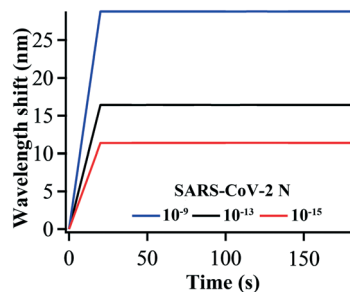

Fig. 7 Sensor response time for the spectrum valley wavelength stabilization.

actual clinical measurement, the RNA-AP sensor distinguishes the low concentration N protein solution (10^{-7} M) and high concentration interference component protein (L-asparagine (ASN) (10^{-3} M), L-citrulline (Cit) (10^{-3} M), urea (10^{-3} M), BSA (10^{-5} M)). The DNA-AP sensor distinguishes the low concentration N protein solution (10^{-11} M) (due to the limitation of the surface area of the microfiber, and the antibody attached to the surface of the fiber can be saturated) and high concentration interference component ASN (10^{-3} M), Cit (10^{-3} M), urea (10^{-3} M) and BSA (10^{-5} M).

As can be seen from Fig. 8A, for the RNA-AP probe, the wavelength shift caused by the N protein is about 45.04 nm, while the weak optical signal responses are caused by Asn, Cit, urea and BSA (with shifts of about 5.44, 19.12, 9.68, and 0.32 nm). It can be seen from Fig. 8B that for the DNA-AP, the wavelength shift caused by the N protein is about 46.40
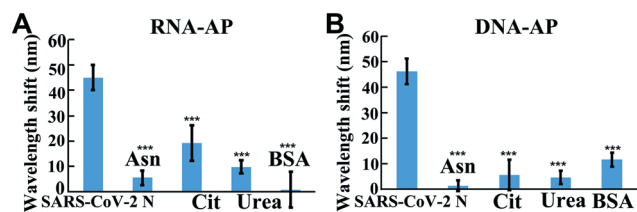
Fig. 8 Comparison of the optical responses of the sensors to (A) 10^{-11} M (RNA-AP) and (B) 10^{-7} M (DNA-AP) N-protein solutions, and potential interference with high concentration ASN (10^{-3} M), Cit (10^{-3} M), urea (10^{-3} M) and BSA (10^{-5} M). ($n = 3$), ***$P < 0.001$.

nm, which is bigger than the optical responses caused by Asn, Cit, urea and BSA (with shifts of about 1.28, 5.52, 4.56, and 11.52 nm). The significant spectral response of the RNA-AP and DNA-AP to the N protein proves the adaptability and selectivity of the aptamers to the SARS-CoV-2 N protein.

Detection of the N protein in fetal bovine serum

In order to prove the feasibility of this sensing method in clinical applications, we used this sensor to detect the N protein mixed in fetal bovine serum samples. The test platform faces the challenge of a complex sample matrix, similar to the situation encountered when analyzing human serum or other biological fluids. In this test, the sensor reacts with the serum without the N protein and FBS with the N protein for 3 minutes, which is the detection time, and then it is washed for 5 minutes after each reaction. The results indicate that the resonance wavelength of the sensor has a small red-shift when it reacts with the serum, but a large red-shift happens when it reacts with the N protein serum. Among them, when the RNA-AP sensor detects bovine serum albumin, the shift is 8.52 nm, and the shift is 34.4 nm if reacting with the N protein (1×10^{-9} M) in FBS (Fig. 9A). When the DNA-AP sensor detects bovine serum albumin, the shift is 19.92 nm while it is 48.72 nm if reacting with the N protein in FBS (Fig. 9B). The small red-shift of bovine serum albumin detected by the sensors may be due to the direct capture by the GO coating, since the aptamers could not completely cover the GO coating even though we incubated the optical fiber with the aptamers for up to 2 hours. The experimental results show that the presented biosensor has great application potential for the rapid and effective detection of the N protein in a complex sample matrix.

Discussion

We performed SPR and EMSA and confirmed that SARS-CoV N protein's DNA and RNA aptamers were also suitable for the SARS-CoV-2 N protein. Based on this, an *in vitro* detection method was provided here, using a graphene oxide enhanced optical microfiber. This extracellular detection method could avoid cell invasion and cytotoxicity. The optical microfiber can be used for real-time quantitative analysis of molecular adsorption on its surface, because its refractive index (RI) can
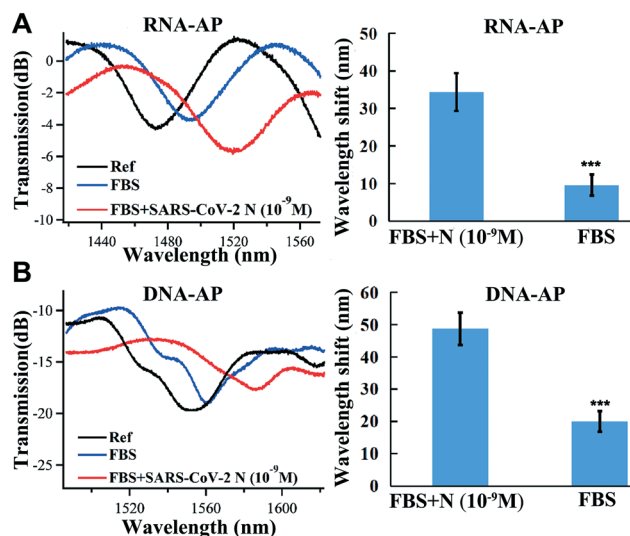

Fig. 9 Transmission spectra and wavelength shift histogram of the microfiber sensors with the (A) RNA-AP@GO and (B) DNA-AP@GO nanointerfaces responding to FBS with and without the N protein. ($n = 3$), ***$P < 0.001$.

be adjusted by the adsorbed molecules.[27] Putting the optical fiber in the SARS-CoV-2 N protein solution, the aptamers capturing the SARS-CoV-2 N protein on the surface of the optical microfiber would cause changes in surface roughness and thickness. It was found that after the protein was captured, the surface roughness and thickness of the fiber increased significantly, changing the surface effective refractive index and causing the frequency shift of the spectrum. Owing to their advantages of miniature size, light weight, portability, short response time, electromagnetic immunity and mechanical flexibility, optical microfibers are suitable for integration with current analytical tools for sensing applications in inaccessible locations,[20] which can also provide great potential for *in situ* monitoring and analysis in a real matrix.[12] In order to improve the sensor sensitivity and reduce the detection limit to meet the detection requirements, we constructed a functionalized graphene oxide nanointerface. Due to the structural and electronic, optical and biochemical properties of graphene oxide,[28–30] more bioprobe molecules are immobilized, and the LOD of the prepared sensor is 6.25×10^{-19} M. Such a low LOD sensor could provide a good platform for virus detection. The sensor was used to detect a variety of proteins, and the results show that it has high selectivity, which benefits from the binding properties of the probes and the SARS-CoV-2 N protein. We also proved the feasibility of this sensing method in clinical applications, and we used this sensor to detect the N protein mixed in FBS samples, similar to the situation encountered when analyzing human serum or other biological fluids. Since the pH value of FBS (pH = 7.4) is similar to that of human serum (pH = 7), this sensor structure can detect the presence of the actual SARS-CoV-2 N protein.[31] The detection sensitivity reaches 1×10^{-9} M. Recently, more and more new sensors for detecting SARS-

CoV-2 have been researched. The comprehensive summary of multiple mature detection methods and new detection methods is presented in Table S1 in the ESI.† Among these methods, the current sensor has advantages in detection limit and detection time. However, the optical microfiber is slightly fragile and the antibody attached to the surface of the fiber can be easily saturated, which limits the detection range and could be improved with the integration of a microfluidic chip. Further, the repeatability of the sensor probe can be improved by controlling the parameters of the tapered fiber preparation, the probe incubation environment and the detection environment. Nevertheless, the above results suggest that this approach can be utilized for quantitative monitoring of coronavirus particles due to its high sensitivity, which can help to quickly exclude patients who do not have the infection.

Conclusions

In conclusion, the corresponding nucleotide sequences of the SARS-CoV-2 N protein were synthesized and cloned into His vectors for expression in *E. coli*, and the expressed N protein was purified by affinity chromatography. We performed SPR and EMSA and confirmed that SARS-CoV N protein's DNA and RNA aptamers were also suitable for the SARS-CoV-2 N protein. To verify the ability of the nucleic acids for protein capture, an optical microfiber sensor with a GO nanointerface was proposed for real-time monitoring of the SARS-CoV-2 N protein. A low LOD of 6.25×10^{-19} M can be obtained. We also proved the feasibility of this sensing method in clinical applications, and used this sensor system to detect the N protein mixed in FBS samples, similar to the situation encountered when analyzing human serum or other biological fluids. The detection sensitivity reaches 1×10^{-9} M. Such an ultra-low detection limit and miniaturized sensor with a high sensitivity could detect ultra-low concentrations of protein *in vitro*, which can be used to quickly exclude patients who do not have the infection. However, due to the ultra-fine waist diameter of the tapered fiber, the antibody attached to the fiber surface can be easily saturated, which limits the upper limit of detection. Thus, it needs to be cleaned after saturation, and the same microfiber sensor can be used for a limited number of times. Such a kind of sensor can also be changed to other optical fiber interface to meet different detection targets, providing a direction for more biological detection.

Author Contributions

Hao Jia: conceptualization, methodology, investigation, supervision, review & editing, project administration, and funding acquisition; Ao Zhang: conceptualization, methodology, investigation, validation, formal analysis, and writing-original draft; Yuquan Yang: conceptualization, investigation, and writing; Yaqi Cui: conceptualization, supervision, writing, and editing; Jianrong Xu: conceptualization, supervision, and review & editing; Hewei Jiang: methodology, investigation, validation, and editing; Shengce Tao: methodology, investigation, validation, and editing; Dawei Zhang: conceptualization, supervision, and writing-review & editing; Heping Zeng: conceptualization, supervision, and writing-review & editing; Zhaoyuan Hou: conceptualization, supervision, and writing-review & editing; Jijun Feng: conceptualization, supervision, writing-review & editing, project management, and funding acquisition. Hao Jia and Ao Zhang contributed equally. All the authors have given approval to the final version of the manuscript.

Conflicts of interest

The authors declare no conflict of interest.

Acknowledgements

References

1 Y. Yang, F. Peng, R. Wang, M. Yange, K. Guan, T. Jiang, G. Xu, J. Sun and C. Chang, *J. Autoimmun.*, 2020, **109**, 102434.

2 B. Udugama, P. Kadhiresan, H. N. Kozlowski, A. Malekjahani, M. Osborne, V. Y. C. Li, H. Chen, S. Mubareka, J. B. Gubbay and W. C. W. Chan, *ACS Nano*, 2020, **14**(4), 3822–3835.

3 F. Xiang, X. Wang, X. He, Z. Peng, B. Yang, J. Zhang, Q. Zhou, H. Ye, Y. Ma, H. Li, X. Wei, P. Cai and W. L. Ma, *Clin. Infect. Dis.*, 2020, ciaa461.

4 Y. M. Kamil, M. H. A. Bakar, M. A. Mustapa, M. H. Yaacob, N. H. Z. Abidin, A. Syahir, H. C. Lee and M. A. Mahdi, *Sens. Actuators, B*, 2018, **257**, 820–828.

5 G. Salceda-Delgado, D. Monzon-Hernandez, A. Martinez-Rios, G. A. Cardenas-Sevilla and J. Villatoro, *Opt. Lett.*, 2012, **37**, 1974–1976.

6 G. Salceda-Delgado, A. Martinez-Rios, R. Selvas-Aguilar, R. I. Alvarez-Tamayo, A. Castillo-Guzman, B. Ibarra-Escamilla, V. M. Duran-Ramirez and L. F. Enriquez-Gomez, *Sensors*, 2017, **17**(6), 1259.

7 V. Ahsani, F. Ahmed, M. B. Jun and C. Bradley, *Sensors*, 2019, **19**(07), 1652.

8 J. Wo, G. Wang, Y. Cui, Q. Sun, R. Liang, P. P. Shum and D. Liu, *Opt. Lett.*, 2012, **37**, 67–69.

9 X. Wang and O. S. Wolfbeis, *Anal. Chem.*, 2016, **88**, 203–227.

10 K. Li, G. Liu, Y. Wu, P. Hao, W. Zhou and Z. Zhang, *Talanta*, 2014, **120**, 419–424.

11 S. H. K. Yap, K. K. Chan, G. Zhang, S. C. Tjin and K. T. Yonget, *ACS Appl. Mater. Interfaces*, 2019, **11**(31), 28546–28553.

12 A. Xiao, Y. Huang, J. Zheng, P. Chen and B. Guan, *ACS Appl. Mater. Interfaces*, 2020, **12**, 1799–1805.

13 S. Kumar, R. Singh, G. Zhu, Q. Yang, X. Zhang, S. Cheng, B. Zhang, B. K. Kaushik and F.-Z. Liu, *IEEE Trans. NanoBiosci.*, 2019, **19**(2), 173–182.

14 C. Liu, Q. Cai, B. Xu, W. Zhu, L. Zhang, J. Zhao and X. Chen, *Biosens. Bioelectron.*, 2017, **94**, 200–206.

15 H. W. Jiang, Y. Li, H. N. Zhang, W. Wang, X. Yang, H. Qi, H. Li, D. Men, J. Zhou and S. C. Tao, *Nat. Commun.*, 2020, **11**(1), 3581.

16 Y. M. Kamil, S. H. Al-Rekabi, M. H. Yaacob, A. Syahir, H. Y. Chee, M. A. Mahdi and M. H. A. Bakar, *Sci. Rep.*, 2019, **9**(1), 1–10.

17 Y. Wu, P. Xue, Y. Kang and K. M. Hui, *Anal. Chem.*, 2013, **85**(6), 3166–3173.

18 P. Saengdee, W. Chaisriratanaku, W. Bunjongpru, W. Sripumkhai, A. Srisuwan, W. Jeamsaksiri, C. Hruanun and A. Poyai, *Biosens. Bioelectron.*, 2015, **67**, 134–138.

19 Z. Cao, B. Yao, C. Qin, R. Yang, Y. Guo, Y. Zhang, Y. Wu, L. Bi, Y. Chen, Z. Xie, G. Peng, S. Huang, C. Wong and Y. Rao, *Light: Sci. Appl.*, 2019, **8**, 107.

20 H. Li, Y. Huang, C. Chen, A. Xiao, G. Hou, Y. Huang, X. Feng and B. O. Guan, *Adv. Sci.*, 2018, **5**(8), 1701074.

21 S. Kumar, R. Singh, Q. Yang, S. Cheng, B. Zhang and B. K. Kaushik, *IEEE Sens. J.*, 2020, **21**(1), 62–70.

22 D. G. Ahn, I. J. Jeon, J. D. Kim, M. S. Song, S. R. Han, S. W. Lee, H. Jung and J. W. Oh, *Analyst*, 2009, **134**(9), 1896–1901.

23 K. T. Shum and J. A. Tanner, *ChemBioChem*, 2008, **9**(18), 3037–3045.

24 http://unafold.rna.albany.edu/?q=mfold.

25 B. K. Kaushik, L. Singh, R. Singh, G. Zhu, B. Zhang, Q. Wang and S. Kumar, *IEEE Trans. NanoBiosci.*, 2020, **19**(3), 477–484.

26 L. Singh, R. Singh, S. Kumar, B. Zhang and B. K. Kaushik, *IEEE J. Quantum Electron.*, 2020, **56**(4), 7700208.

27 B. Yu, Y. Y. Huang, J. Zhou, T. A. Guo and B. O. Guan, *Talanta*, 2017, **165**, 245–250.

28 C. Gomez, E. Robalino, D. Haro, T. Tene, P. Escudero, A. Haro and J. Orbe, *Mater. Today*, 2016, **3**(3), 796–802.

29 S. Dave, C. Gong, A. Robertson, J. Warner and C. Grossman, *ACS Nano*, 2016, **10**, 7515–7522.

30 K. Loh, Q. Bao, G. Eda and M. Chhowalla, *Nat. Chem.*, 2010, **2**, 1015–1024.

31 L. Singh, R. Singh, B. Zhang, B. K. Kaushik and S. Kumar, *IEEE Trans. Nanotechnol.*, 2020, **21**, 201–208.